



Obrabotka metallov -

Metal Working and Material Science

Journal homepage: http://journals.nstu.ru/obrabotka_metallov







The effect of technological parameters on the microstructure and properties of the AlSiMg alloy obtained by selective laser melting

Natalia Saprykina^{1, a, *}, Alexandr Saprykin^{1, b}, Yurii Sharkeev^{2, c}, Egor Ibragimov^{1, d}

¹ National Research Tomsk Polytechnic University, 30 Lenin Avenue, Tomsk, 634050, Russian Federation

² Institute of Strength Physics and Materials Sciences SB RAS, 2/4, pr. Akademicheskii, Tomsk, 634055, Russian Federation

^a  <https://orcid.org/0000-0002-6391-6345>,  saprikina@tpu.ru; ^b  <https://orcid.org/0000-0002-6518-1792>,  sapraa@tpu.ru;

^c  <https://orcid.org/0000-0001-5037-245X>,  sharkeev@ispms.tsc.ru; ^d  <https://orcid.org/0000-0002-5499-3891>,  egor83rus@tpu.ru

ARTICLE INFO

Article history:

Received: 05 June 2024

Revised: 17 June 2024

Accepted: 28 June 2024

Available online: 15 September 2024

Keywords:

Selective laser melting

Metal Powder

Porosity

Scanning strategy

Modes of selective laser melting

Microhardness

Energy deposition

Aluminum-silicon-magnesium alloy system

Funding

The research was carried out at the expense of a grant from the Russian Science Foundation No. 22-29-01491, <https://rscf.ru/project/22-29-01491/>

Acknowledgements

Authors would like to thank to Ph.D. M.A. Khimich, Ph.D. V.V. Chebo-daeva, I.A. Glukhov for their help in conducting research. The equipment of the NMNT TPU Central Control Center was used in the work.

ABSTRACT

Introduction. The development of additive technologies is aimed at the synthesis of new powder compositions for selective laser melting plants, the study of the effect of mode parameters on the stable quality of products. **The purpose of this work** is to study the effect of the scanning strategy on the microstructure, elemental composition, porosity and density of specimens obtained by selective laser melting from non-spherical powders (*Al* — 91 wt. %, *Si* — 8 wt. %, *Mg* — 1 wt. %), subjected to special preparation to determine the optimal conditions for selective laser melting. **The research methods** are methods of X-ray diffraction and X-ray phase analysis, transmission electron microscopy. The paper examines specimens formed using four different scanning strategies. **Results and discussions.** A promising aluminum alloy *AlSi8Mg* is developed for selective laser melting. The material has good manufacturability and low powder cost. The technological parameters of melting make it possible to form a thin structure with a low level of porosity. The mechanism of influence of the scanning strategy on porosity, surface morphology, relative density and microstructure is investigated. A specimen from the *AlSi8Mg* powder composition with a high relative density of 99.97 % is produced by selective laser melting with an energy density of 200 J/mm³, a specimen scanning circuit when the direction of laser movement changes by an angle of 90° each odd layer. It is proved that the density of the *AlSiMg* alloy depends on the scanning strategy used. The calculated density of the specimen was 2.5 g/cm³, which corresponds to the density of silumin. Analysis of *SEM* images and maps of the distribution of elements (*Al*, *Mg*, *Si*) of the specimens showed that different specimen formation strategies do not affect the nature of silicon distribution. A unique grain structure is observed in the resulting *AlSi8Mg* alloy. The melt pool consists of small grains along the border and large grains in the center. The formation of fine grains is explained by the addition of *Si* and the high cooling rate during selective laser melting.

For citation: Saprykina N.A., Saprykin A.A., Sharkeev Y.P., Ibragimov E.A. The effect of technological parameters on the microstructure and properties of the AlSiMg alloy obtained by selective laser melting. *Obrabotka metallov (tekhnologiya, oborudovanie, instrumenty) = Metal Working and Material Science*, 2024, vol. 26, no. 3, pp. 192–207. DOI: 10.17212/1994-6309-2024-26.3-192-207. (In Russian).

* Corresponding author

Saprykina Natalia A., Ph.D. (Engineering), Associate Professor
National Research Tomsk Polytechnic University,
30 Lenin Ave.,
634050, Tomsk, Russian Federation
Tel.: +7 923 49-72-483, e-mail: saprikina@tpu.ru

Introduction

Selective laser melting (*SLM*) is an additive manufacturing (*AM*) technology in which metal powder is melted by a laser beam along a given trajectory to make products layer by layer. Compared with traditional manufacturing technologies, *SLM* has a number of advantages, such as rapid prototyping, production of complex-shaped parts and reduced lead time. The technology is developing towards synthesizing new powder compositions for *SLM* units, studying the influence of mode parameters upon the stable quality of the products, repeatability and reproducibility of the process on different devices [1].

Aluminum and aluminum-based powders are some of the most common materials in the automotive, aerospace and aviation industries due to its excellent strength-to-weight ratio, good thermal and electrical conductivity, and corrosion resistance. Recently, aluminum-based powder has also been the object of research for use in selective laser melting units [2]. This technology allows not only to shorten the design and production cycle, but also to obtain an alloy with a unique structure as metal powder is rapidly melted and cooled [3].

Currently, there are many studies concerning production of various items from aluminum-based powders using the *SLM* technology [4–6], and recommendations are given to improve the quality of the resulting products. Thus, when determining the *SLM* conditions, the following physical properties of aluminum are taken into account: high thermal expansion coefficient, high shrinkage during solidification, low level of laser energy absorption, formation of strong oxide layer, high thermal conductivity, relatively wide range of solidification temperatures [7–9]. Defects of the surface and internal structure, such as porosity, layer distortion, cracking, low dimensional accuracy and surface roughness occurred in the process of selective laser melting of aluminum-based powders [10]. These defects are often associated with development of uneven temperature gradients along the fused surface, with contamination of powder by oxides, with inhomogeneity of surface tension which prevents the adhesion of the melt to the substrate and interlayer bonding [11]. All the studies were completed on the specimens produced from the special spherical powders of the necessary alloys which cost a lot. The relative density of the specimens made from spherical powders is over 99.5 %. It was obtained by optimizing laser scanning parameters from *AlSi10Mg* [12], [13], *Al-12Si* [14] and *AlSi7Mg* [15] alloys. In addition, these specimens showed excellent mechanical properties of the formed fine cellular dendrite microstructure, which results from the *SLM* process [16]. Despite the advances in the field of additive technologies, only a limited number of aluminum alloys can be used to produce a high-quality product using the *SLM* method [17]. Completely dense and crack-free specimens from aluminum-based powders can be produced using *SLM* in a narrow range of modes [18, 19], which is selected experimentally for each material. The research for non-spherical powders has not been described by scientists.

The *SLM* conditions include over 120 parameters that, to one degree or another, affect the quality of the resulting product. Beside the selective laser melting mode the scanning strategy is also one of the processing parameters that affects the microstructure formation and the properties of the resulting products. By controlling the direction of the heat flow between the layers through the laser beam scanning strategy it is possible to form various grain structures and change the direction of the interlayer grains growth [20]. High energy consumption and uneven temperature distribution lead to huge temperature gradients, high thermal stresses and deformation. Thermal temperature gradients, direction of the heat flow and the cooling rate have a very important influence upon the dislocation density, grain size and texture of the manufactured products.

The purpose of the given paper is to study the influence of the scanning strategy on the microstructure, elemental composition, porosity and density of the specimens produced by selective laser melting from non-spherical powders (*Al* – 91 wt. %, *Si* – 8 wt. %, *Mg* – 1 wt. %) specially prepared as described in the previously published papers [21] to determine optimal *SLM* conditions.

This purpose requires solving the following problems: producing specimens from the prepared powder composition [21] using the selective laser melting method with different scanning strategies; identifying of the optimal scanning strategy, which allows producing a specimen with the lowest porosity without changing other melting parameters; determining the density of the specimens, studying the structural and phase composition of the specimen using the transmission microscopy method.

Research methods

The research was carried out on a 3D printer *VARISKAF-100MVS* manufactured in Yurga Institute of Technology of Tomsk Polytechnic University. The unit is equipped with a 100 W ytterbium fiber laser with a wavelength of 1,070 nm. The process of formation and study of the *AlSiMg* powder from single-component powders of aluminum, silicon and magnesium was described previously in [21]. To analyze the influence of the scanning strategy on the microstructure, elemental composition, porosity and density of the specimens the conditions were determined by search experiments and described in the paper [22]. Specimens with a size of 10×10×3 mm were produced under the following mode parameters: scanning speed $V = 225$ mm/s, scanning step $S = 0.08$ mm, laser power $P = 90$ W, powder layer thickness $h = 0.025$ mm. The temperature of the working table at the beginning of the *SLM* cycle was +25 °C; the powder was melted in the protective argon environment. An energy density of 200 J/mm³ provided sufficient heat to melt the powder and promoted the remelting of the part of the previous layer and melt path to smoothly connect the adjacent layers [22]. After formation the specimens were ground and polished using diamond pastes, removing 400 μm of the top layer. Porosity was determined as the average value from nine optical images of the polished section surface. The shooting pattern is shown in Figure 1.

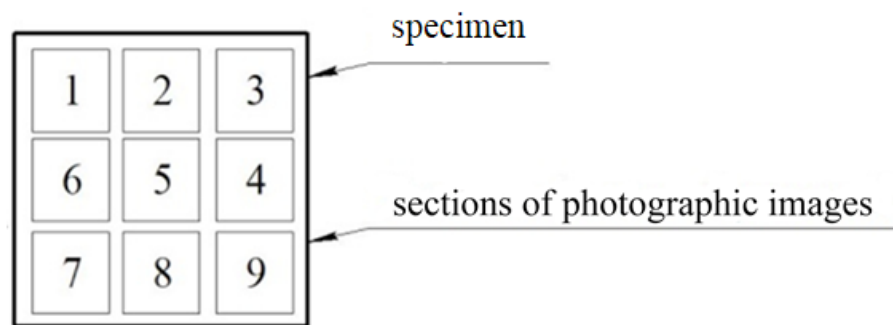


Fig. 1. Shooting pattern

Studies of the structural-phase state of the specimen were completed using a transmission electron microscope *JEOL JEM-2100*. Shooting conditions were as follows: accelerating voltage of 200 kV, magnification of 6,000–1,500,000 times, “column length” under the microdiffraction mode of 100 cm. The phase identification was carried out using the international card database *ICDDPDF4+* (International Center for Diffraction Data).

To study the effect of scanning strategy on the microstructure and porosity of the specimens, four strategies were implemented. Scanning strategy I ($\angle 90^\circ$), in which the direction of laser movement changes by an angle of 90° from layer to layer, is shown in Figure 2. (See the marks below)

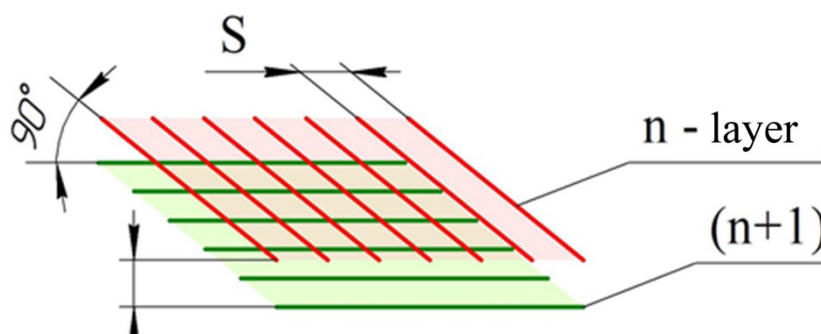


Fig. 2. Scanning strategy I ($\angle 90^\circ$)

With scanning strategy II ($\angle 45^\circ$) the direction of laser movement changes by an angle of 45° from layer to layer, see Figure 3.

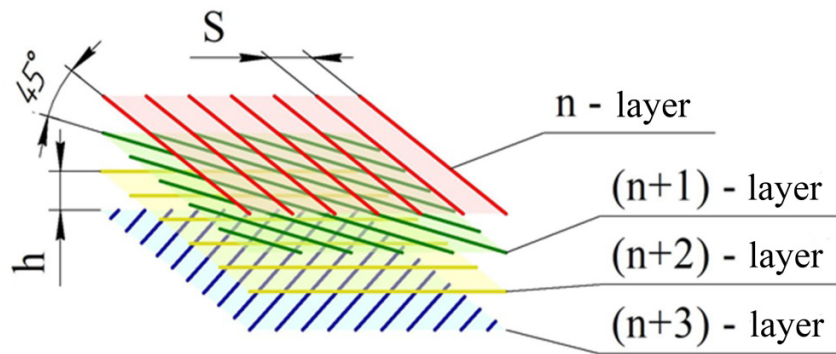


Fig. 3. Scanning strategy II ($\angle 45^\circ$)

With scanning strategy III ($\angle 90S/2$), the specimen is formed when the direction of the laser movement changes by 90° every odd layer ($n, n+2$, etc.). In every even layer ($n+1, n+3$), the direction of the laser beam is parallel to the previous layer, and the track is shifted by a distance of $S/2$. The strategy is shown in Figure 4.

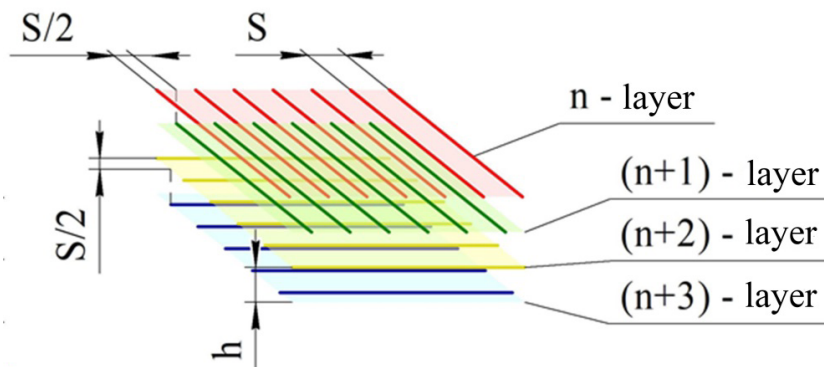


Fig. 4. Scanning strategy III ($\angle 90S/2$)

Scanning strategy IV ($\angle 90p.p.$), in which each layer is scanned by the laser beam twice (double remelting) and during the second pass the step is shifted by $S/2$ while the direction of the laser movement changes by 90° from layer to layer. This scheme is shown in Figure 5.

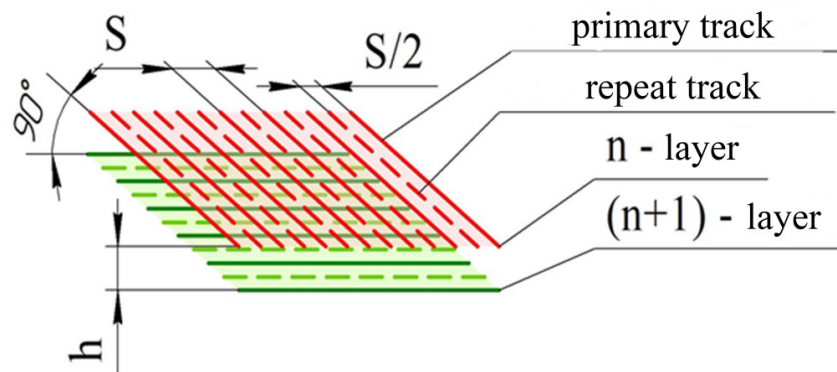




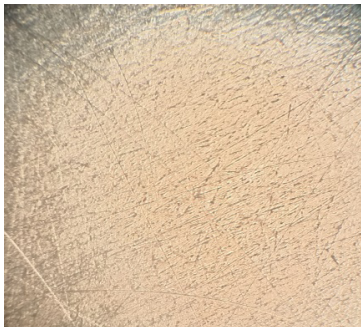

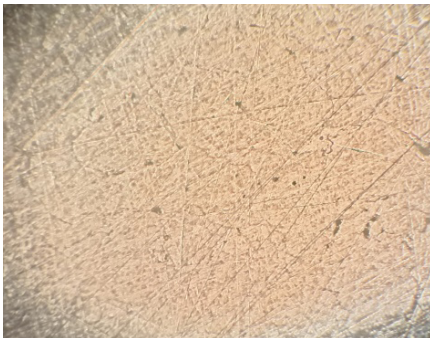
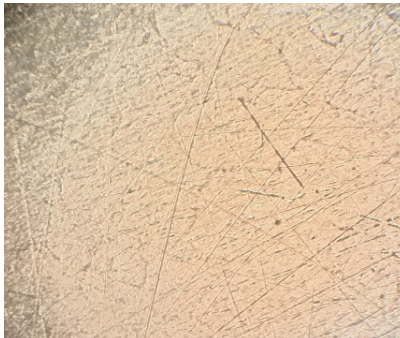
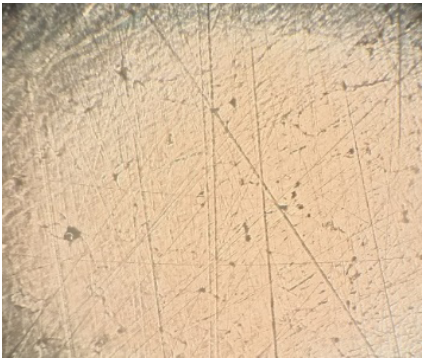

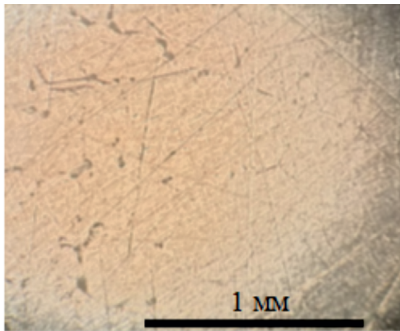


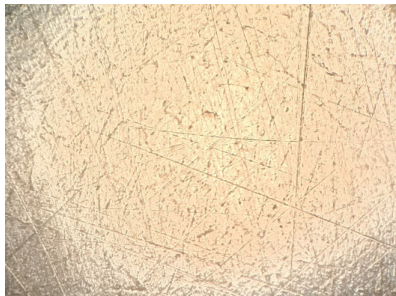
Fig. 5. Scanning strategy IV ($\angle 90 p.p.$)

Results and discussion

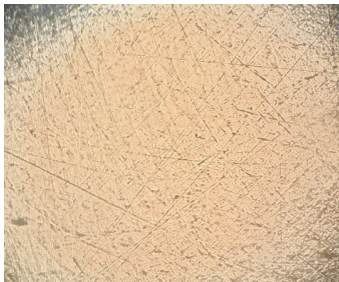
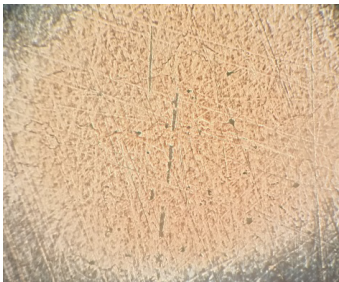
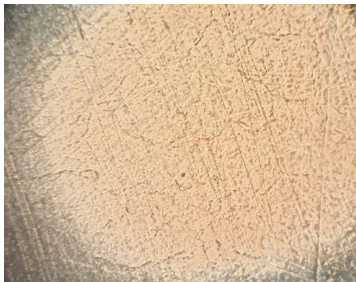
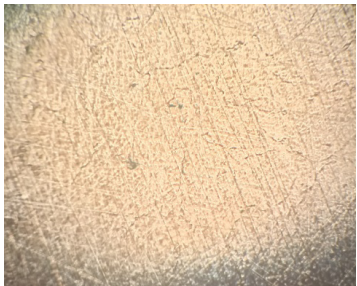
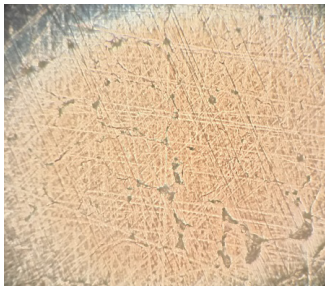
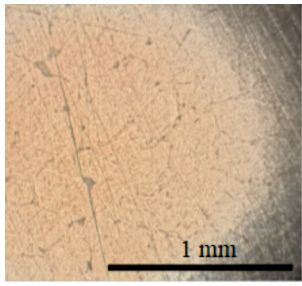

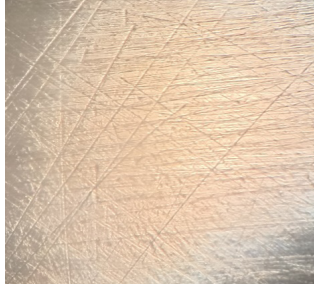
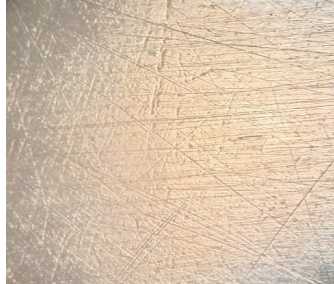
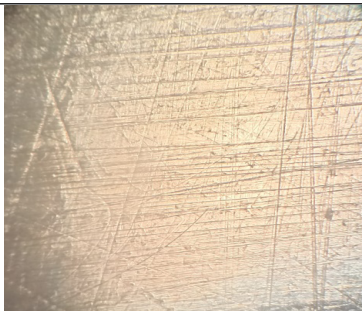
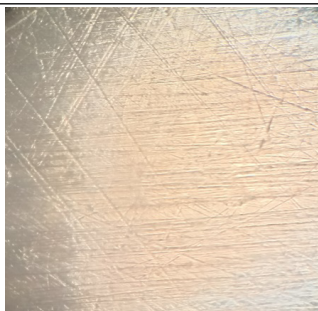

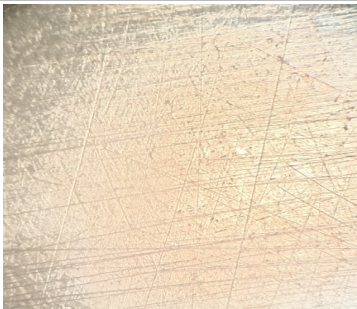
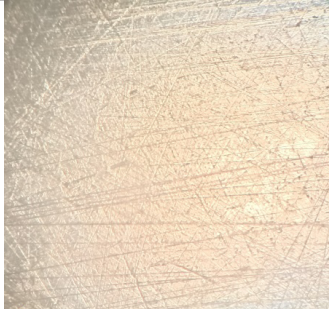
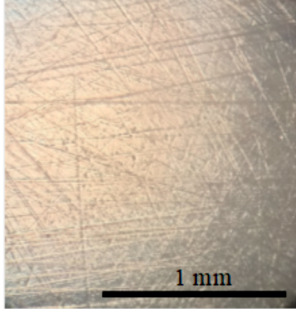
The photographs of the structure of the specimens formed with the use of different scanning strategies from the composition of powders under the following SLM modes [22]: $P = 90$ W; $v = 225$ mm/s; $S = 0.08$ mm; $h = 0.025$ mm; $t = 25$ C°, are presented in Table 1.

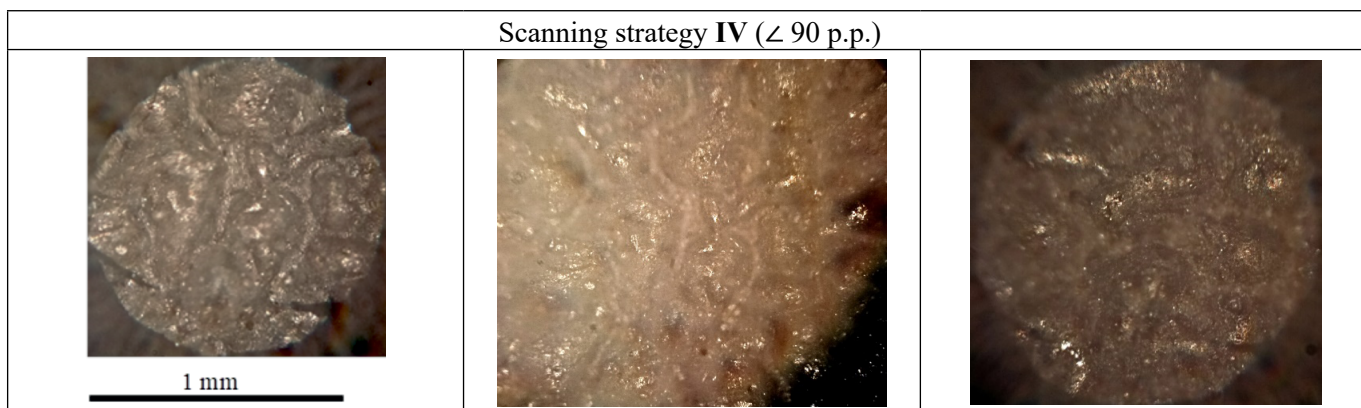
Table 1

Photos of the specimen structure and porosity values, %

Scanning strategy I ($\angle 90$)		
		
0.01	0.02	0.01
		
0.43	0.39	0.06
		
0.63	0.35	0.93
“Average” porosity is 0.31 %		
Scanning strategy II ($\angle 45$)		
		
0.11	0.09	0.05

Continuation of the table 1

		
0.18	0.14	0.06
		
0.11	1.36	0.47
“Average” porosity is 0.29 %		
Scanning strategy III ($\angle 90S/2$)		
		
0.04	0.01	0.02
		
0.06	0.01	0.02
		
0.05	0.04	0.03
“Average” porosity is 0.03 %		



As a result of double remelting large melt drops of 0.2–0.5 mm in size were formed on the surface of the layer which led to uneven application of the next powder layer and appearance of non-melts. For this reason it was not possible to build-up a specimen of the required thickness. For this specimen its porosity was not assessed due to impracticality. The graph of average porosity dependence upon the scanning strategy shows that the specimen obtained using strategy **III** has the lowest porosity value of 0.03 %, see Figure 6.

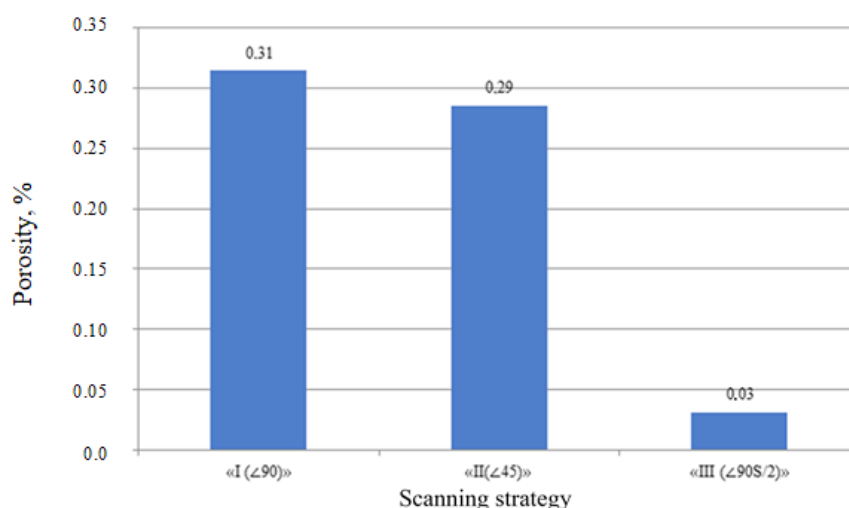


Fig. 6. Dependence of the average porosity of the specimen on the scanning strategy

Density is an important indicator for assessing the quality of the parts. A caliper was used to measure the overall dimensions of the specimens: length×width×height, which was 10×10×3 mm accordingly. Using an analytical balance *VST-600/10* we measured the mass of the specimens, which amounted to 0.748 g for the specimen obtained using scanning strategy **I**, and 0.75 g for scanning strategy **II**. The calculated density of the specimens for scanning strategies **I** and **II** was 2.49 g/cm³, and for the specimen obtained using scanning strategy **III**, 2.5 g/cm³, which corresponds to the density of silumin.

Figure 7 shows *SEM* images and element distribution maps (*Al*, *Mg*, *Si*) of the specimens obtained using different strategies.

Aluminum and magnesium are distributed uniformly in all specimens. Silicon in the specimens is distributed in the form of small particles, less than 5 μm in size. Changing the specimen preparation strategy does not change the nature of silicon distribution in the specimens.

The structural-phase state and elemental composition were determined for the specimen formed using scanning strategy **III**.

The specimen under study has a grain structure; the microscopic pores are not detected at the magnifications used.

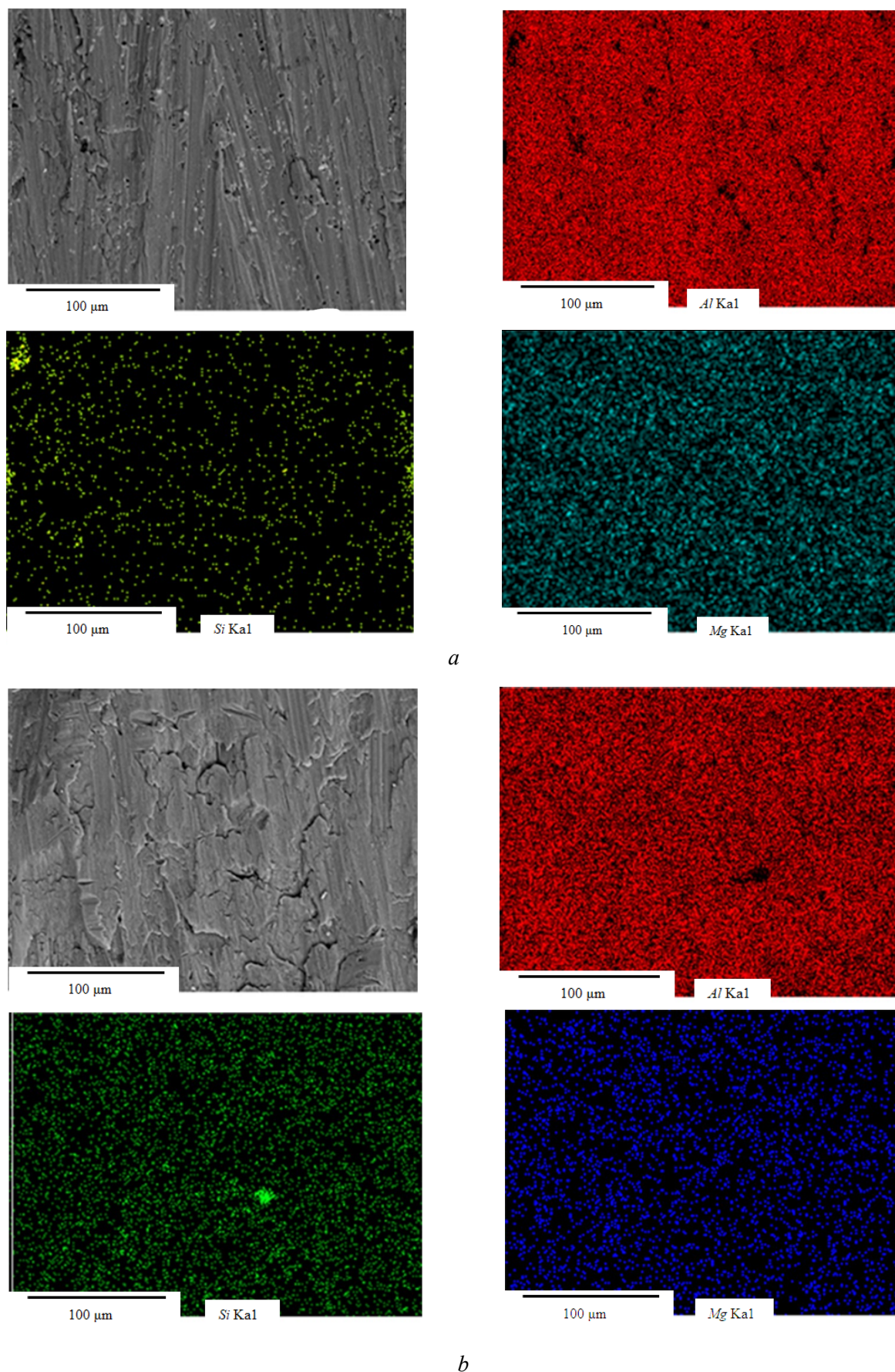
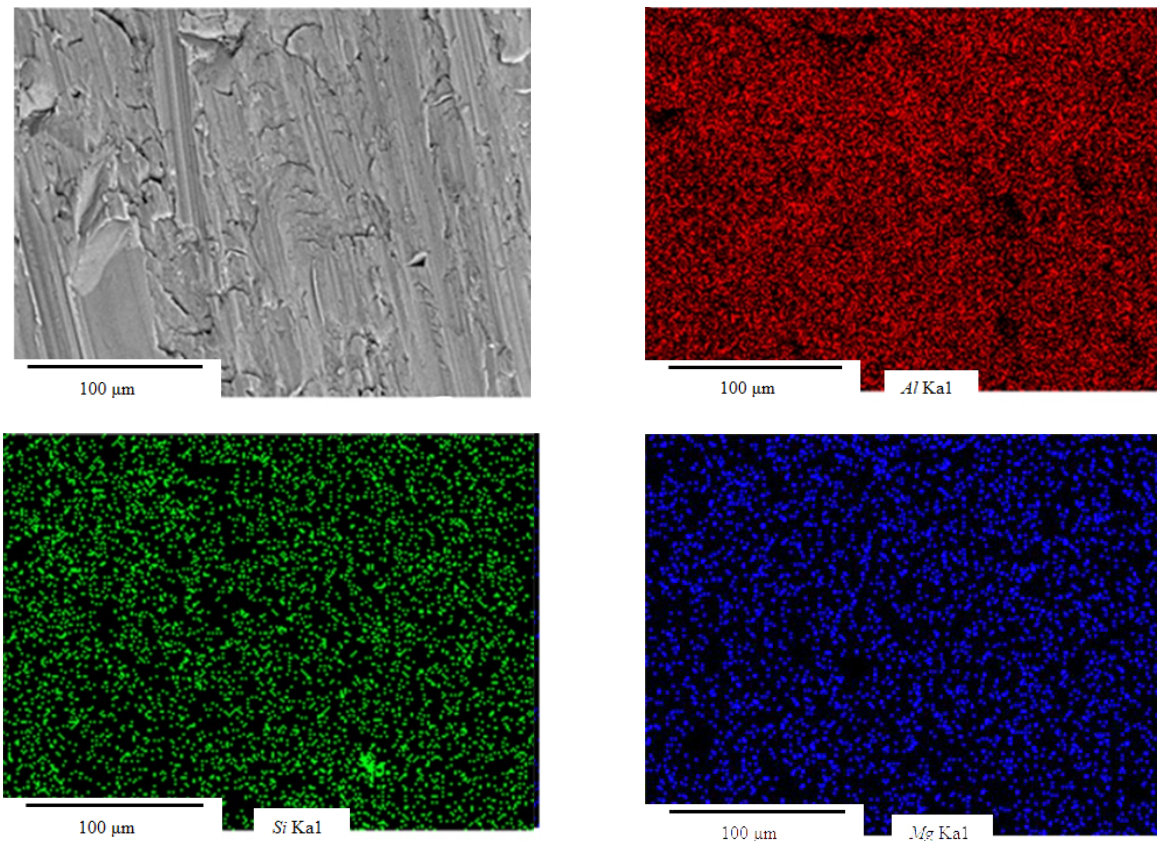


Fig. 7. SEM images and distribution maps of elements (*Al*, *Mg*, *Si*) of specimens using different production strategies:

a – No. 1; *b* – No. 2; *c* – No. 3 (see also next page)



c

Fig. 7. The End

The microdiffraction patterns obtained from different areas are represented, first of all, by reflections of varying intensities. The identified reflections correspond to the *BCC* phase *Al* – 91 wt. %, *Si* – 8 wt. % (*PDF* Card – 04-003-7125). In the microdiffraction pattern, Figure 8 *b*, obtained using the largest field diaphragm at the low magnification of the specimen, there are also reflections located circumferentially which indicates that there are fine particles in the structure of the specimen. At high magnifications and dark-field images it is clearly visible that these fine particles are located at the grain boundaries.

To analyze the homogeneity of element distribution in the specimen under study energy-dispersive microanalysis was used. First of all, element distribution maps throughout the analysis area were built. Mapping showed that the main element of the alloy, *Al*, is distributed evenly in the grains, but its content decreases along the grain boundaries. The second most abundant element, *Si*, on the contrary, is mainly concentrated along the grain boundaries. The third element in terms of content, *Mg*, is distributed evenly throughout the volume under study. Based on the nature of the total spectrum, Figure 9, no other elements are detected in the specimens. The elemental composition of the area under study is presented in Table 2.

To confirm the local heterogeneity of the element composition we also completed the study of elemental composition along a given line. The results of the study are shown in Figure 10. The nature of elements distribution is similar to that of the mapping: at the grain boundaries we observe reduced *Al* and increased *Si* content. As can be seen the concentration of *Mg*, when studied using this method, is also heterogeneous. However, since the *Mg* content in the composition is low (less than 0.5 wt. % according the data of elemental analysis) this cannot be postulated accurately.

A specimen of a complex geometric shape (Figure 11) was produced from the prepared powder mixture under the obtained optimal *SLM* conditions.

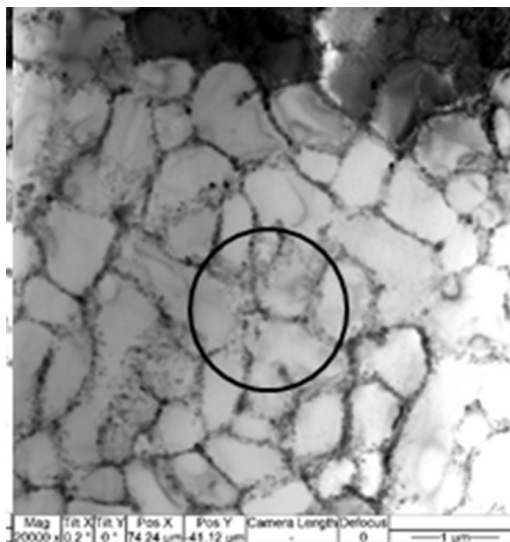
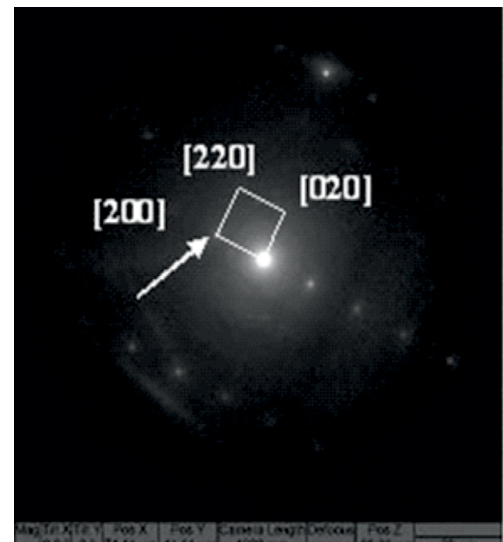
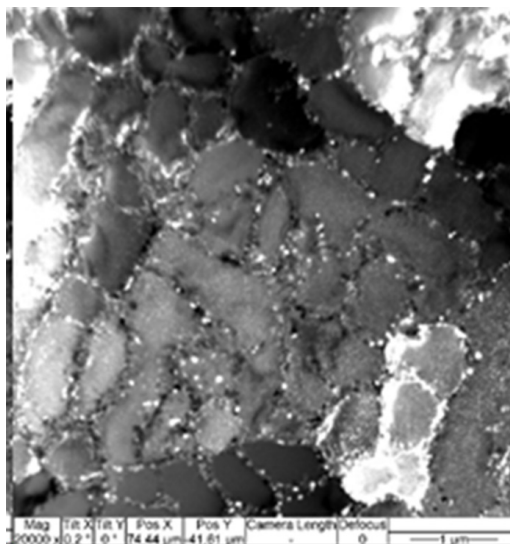
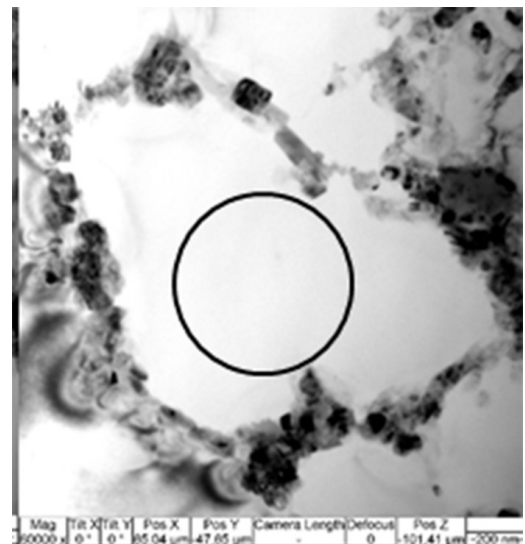
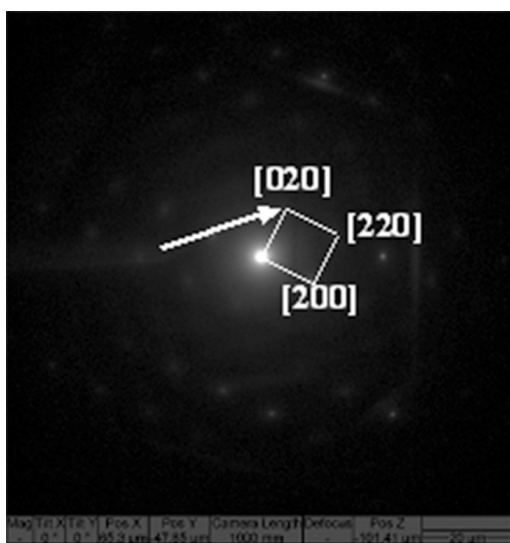
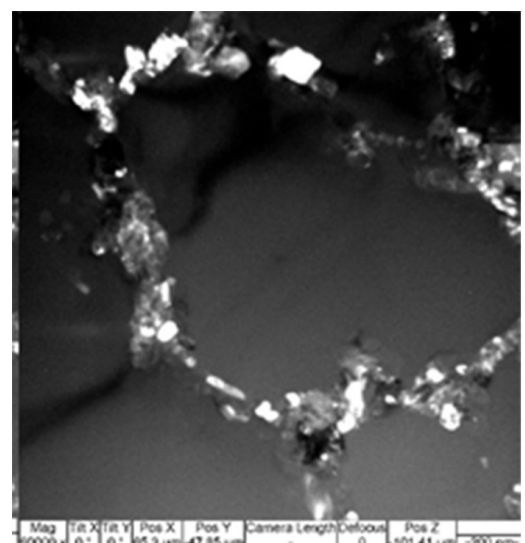
*a**b**c**d**e**f*

Fig. 8. Microstructure of the *AlSiMg* alloy specimen: light-field images (*a*, *d*) with corresponding microdiffraction patterns (*b*, *e*) and dark-field images (*c*, *f*)

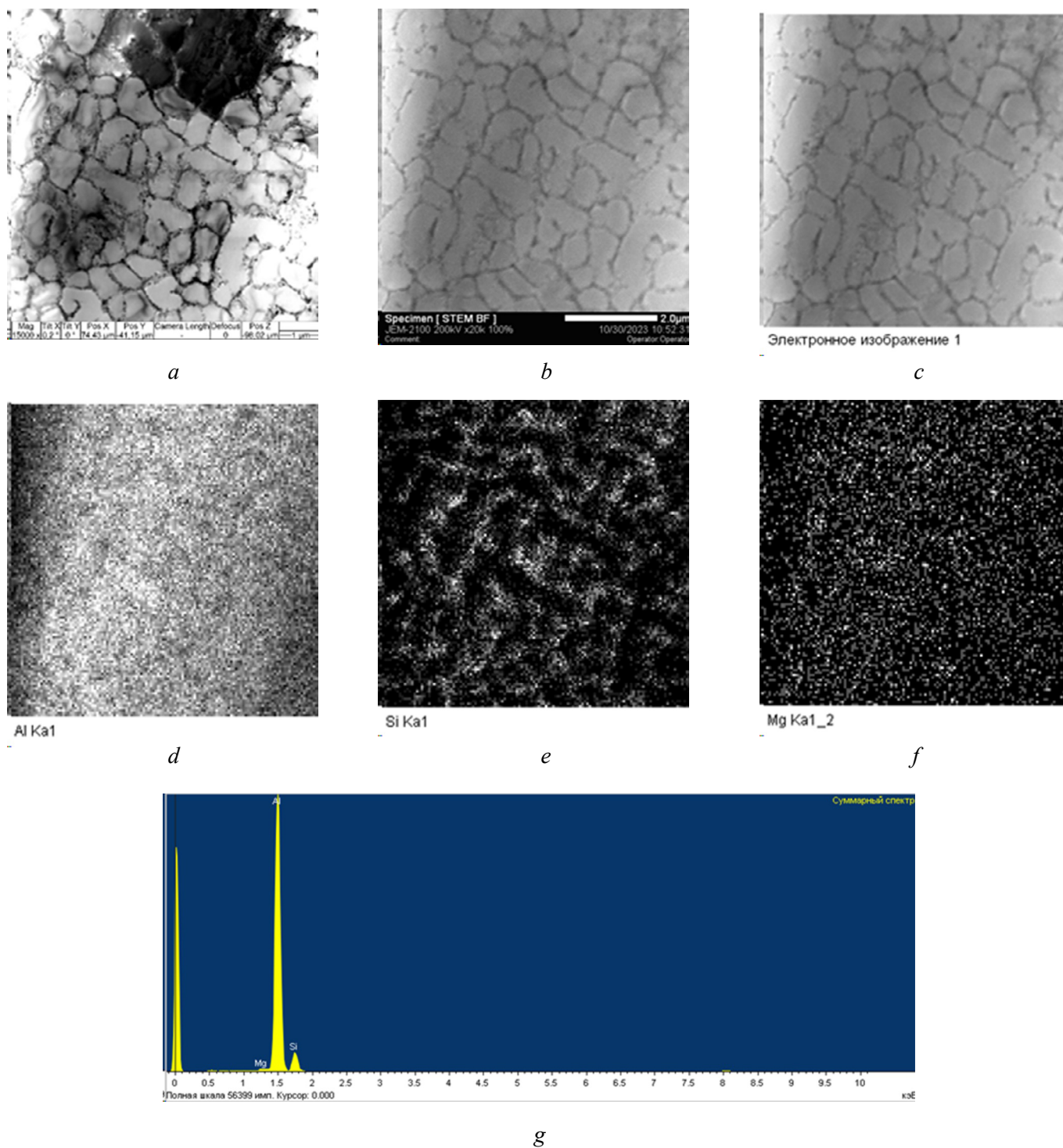


Fig. 9. A bright field image of the analysis area (a), the desired TSM image of the analysis area (b), a TSM image for comparing element maps (c), element distribution maps (d-e) and the total spectrum of the mapping area (g)

Table 2

Elemental analysis of the Al-Si-Mg alloy by the total spectrum from the mapping area

Element	Weight %	Atomic %
Al K	92.65	92.86
Si K	6.95	6.69
Mg K	0.40	0.45

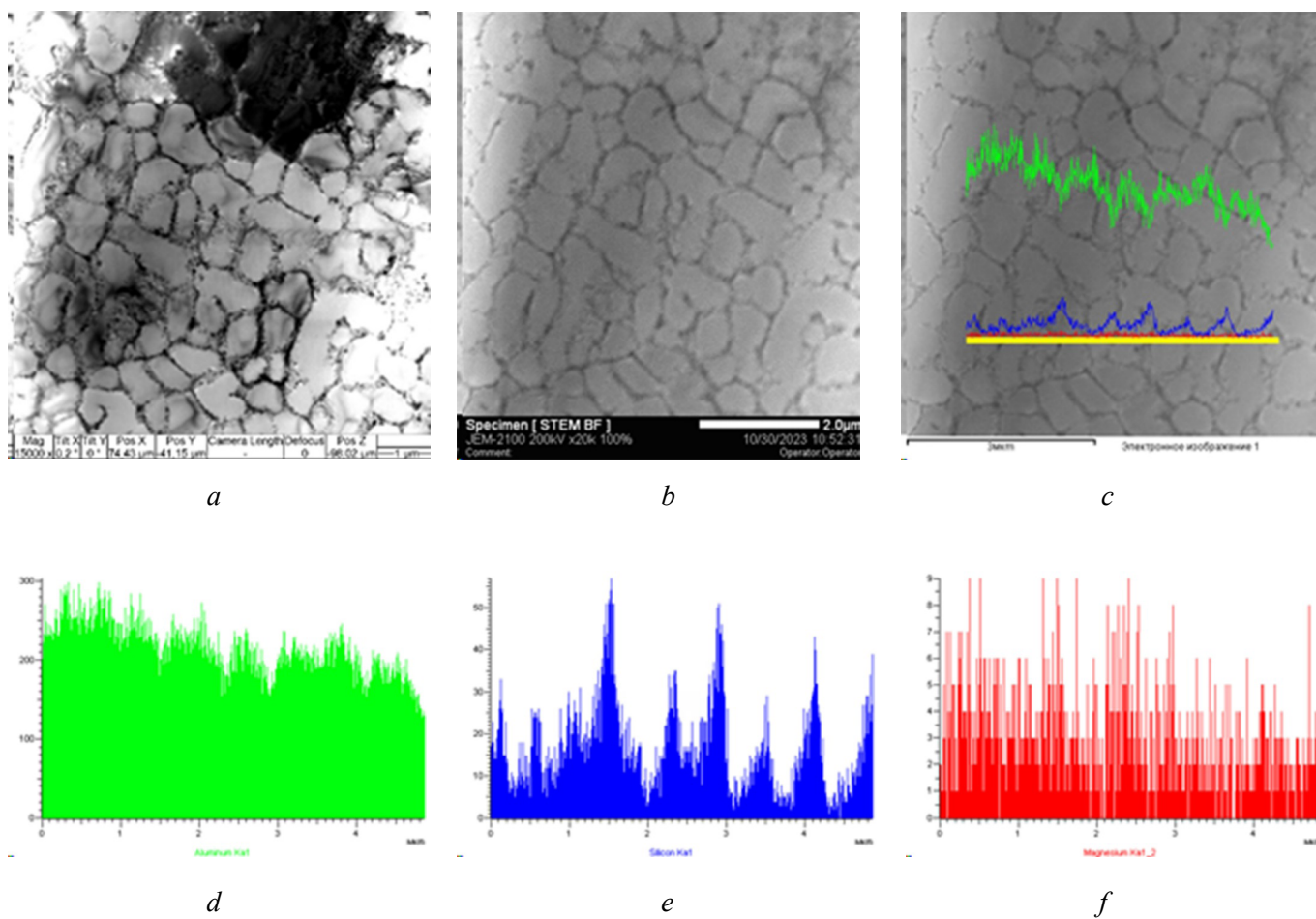


Fig. 10. A bright field image of the analysis area (*a*), the desired TSM image of the analysis area (*b*), a TSM image with plotted element content data (*c*), the distribution of elements along the track (*d*–*f*)



Fig. 11. A prototype of the swirler

Conclusion

In the course of the research, a technology for forming a promising aluminum alloy AlSi8Mg for selective laser melting and non-spherical powders is developed. The material shows good manufacturability and low powder cost. The technological parameters of melting allow forming a fine structure with low porosity. The mechanism of the influence of the scanning strategy on porosity, surface morphology, relative density and microstructure is studied. The main conclusions are summarized as follows.

A specimen was produced from AlSi8Mg powder composition with high relative density of 99.97 % by selective laser melting. The energy density significantly affects the quality of the surface. In this study the energy density of 200 J/mm³ and the specimen formation scanning strategy **III** when the direction of the laser movement changes by 90° every odd layer ($n, n + 2$, etc.) and in every even layer ($n + 1, n + 3$), the direction of the laser beam is parallel to the previous layer, and the track is shifted by a distance of $S/2$ ($\angle 90S/2$) are the best parameters of the process allowing to achieve the highest relative density. It is proven that the density of AlSiMg alloy depends on the scanning strategy used. The calculated density of the specimens for scanning strategies **I** and **II** was 2.49 g/cm³, and for the specimen obtained using scanning strategy **III**, 2.5 g/cm³, which corresponds to the density of silumin.

Analysis of SEM images and element distribution maps (Al, Si, Mg) of the specimens showed that different strategies for producing specimens do not affect the nature of silicon distribution.

Unique grain structure is observed in the finished AlSi8Mg alloy. In the melt pool small grains are located along the boundary, while large grains are in the center. Addition of silicon and high cooling rates are positive conditions for formation of fine grains.

References

1. Oliveira J.P., LaLonde A.D., Ma J. Processing parameters in laser powder bed fusion metal additive manufacturing. *Materials and Design*, 2020, vol. 193 p. 108762. DOI: 10.1016/j.matdes.2020.108762.
2. Kanazawa M., Iwaki M., Minakuchi S., Naoyuki N. Fabrication of titanium alloy frameworks for complete dentures by selective laser melting. *Journal of Prosthetic Dentistry*, 2014, vol. 112 (6), pp. 1441–1447. – DOI: 10.1016/j.prosdent.2014.06.017.
3. Kotadia H.R., Gibbons G., Das A., Howes P.D. A review of laser powder bed fusion additive manufacturing of aluminium alloys: microstructure and properties. *Additive Manufacturing*, 2021, vol. 46, p. 102155. DOI: 10.1016/j.addma.2021.102155.
4. Wang Z.H., Lin X., Kang N., Wang Y.F., Yu X.B., Tan H., Yang H.O., Huang W.D. Making selective-laser-melted high-strength Al-Mg-Sc-Zr alloy tough via ultrafine and heterogeneous microstructure. *Scripta Materialia*, 2021, vol. 203, p. 114052. DOI: 10.1016/j.scriptamat.2021.114052.
5. Geng Y.X., Wang Y.M., Xu J.H., Mi S.B., Fan S.M., Xiao Y.K., Wu Y., Luan J.H. A high-strength Al-SiMg1.4 alloy fabricated by selective laser melting. *Journal of Alloys and Compounds*, 2021, vol. 867, p. 159103. DOI: 10.1016/j.jallcom.2021.159103.
6. Zhang J.L., Gao J.B., Song B., Zhang L.J., Han C.J., Cai C., Zhou K., Shi Y.S. A novel crack-free Ti-modified Al-Cu-Mg alloy designed for selective laser melting. *Additive Manufacturing*, 2021, vol. 38, p. 101829. DOI: 10.1016/j.addma.2020.101829.
7. Shah A.W., Ha S., Kim B., Yoon Y., Lim H., Kim S.K. Effect of Al₂Ca addition and heat treatment on the microstructure modification and tensile properties of hypoeutectic Al–Mg–Si alloys. *Materials*, 2021, vol. 14, p. 4588. DOI: 10.3390/ma14164588.
8. Lefebvre W., Rose G., Delroisse P., Baustert E., Cuvilly F., Simar A. Nanoscale periodic gradients generated by laser powder bed fusion of an AlSi10Mg alloy. *Materials and Design*, 2021, vol. 197, p. 109264. DOI: 10.1016/j.matdes.2020.109264.
9. Bayoumy D., Schliephake D., Dietrich S., Wu X.H., Zhu Y.M., Huang A.J. Intensive processing optimization for achieving strong and ductile Al-Mn-Mg-Sc-Zr alloy produced by selective laser melting. *Materials and Design*, 2021, vol. 198, p. 109317. DOI: 10.1016/j.matdes.2020.109317.
10. Rao J.H., Zhang Y., Zhang K., Huang A., Davies C.H.J., Wu X. Multiple precipitation pathways in an Al-7Si-0.6Mg alloy fabricated by selective laser melting. *Scripta Materialia*, 2019, vol. 160, pp. 66–69. DOI: 10.1016/j.scriptamat.2018.09.045.

11. Zhang H., Gu D., Dai D. Laser printing path and its influence on molten pool configuration, microstructure and mechanical properties of laser powder bed fusion processed rare earth element modified Al-Mg alloy. *Virtual and Physical Prototyping*, 2022, vol. 17, pp. 308–328. DOI: 10.1080/17452759.2022.2036530.
12. Bhattacharjee R., Datta S., Biswas P. Thermomechanical and material flow analysis during friction stir welding of marine grade aluminum alloy 5083. *Journal of Ship Production and Design*, 2023, vol. 39 (1), pp. 1–24. DOI: 10.5957/jspd.02220010.
13. Wei P., Wei Z., Chen Z., Du J., He Y., Li J. Fundamentals of radiation heat transfer in AlSi10Mg powder bed during selective laser melting. *Rapid Prototyping Journal*, 2019, vol. 25 (9), pp. 1506–1515. DOI: 10.1108/rpj-11-2016-0189.
14. Xi L., Wang P., Prashanth K.G., Li H., Prykhodko H.V., Scudino S., Kaban I. Effect of TiB₂ particles on microstructure and crystallographic texture of Al-12Si fabricated by selective laser melting. *Journal of Alloys and Compounds*, 2019, vol. 786, pp. 551–556. DOI: 10.1016/j.jallcom.2019.01.327.
15. Fan H., Witvrouw A., Wolf-Monheim F., Souschek R., Yang S. Effects of substrate surface treatments on hybrid manufacturing of AlSi7Mg using die casting and selective laser melting. *Journal of Materials Science and Technology*, 2023, vol. 156, pp. 142–156. DOI: 10.1016/j.jmst.2023.02.009.
16. Maamoun A.H., Xue Y.F., Elbestawi M.A., Veldhuis S.C. The effect of selective laser melting process parameters on the microstructure and mechanical properties of Al6061 and AlSi10Mg alloys. *Materials*, 2018, vol. 12 (1), p. 12. DOI: 10.3390/ma12010012.
17. Aboulkhair N.T., Simonelli M., Parry L., Ashcroft I., Tuck C., Hague R. 3D printing of aluminium alloys: Additive manufacturing of aluminium alloys using selective laser melting. *Progress in Materials Science*, 2019, vol. 106, p. 100578. DOI: 10.1016/j.pmatsci.2019.100578.
18. Geng Y.X., Wang Y.M., Xu J.H., Mi S.B., Fan S.M., Xiao Y.K., Wu Y., Luan J.H. A high-strength Al-SiMg1.4 alloy fabricated by selective laser melting. *Journal of Alloys and Compounds*, 2021, vol. 867, p. 159103. DOI: 10.1016/j.jallcom.2021.159103.
19. Wu J., Wang X.Q., Wang W., Attallah M.M., Loretto M.H. Microstructure and strength of selectively laser melted AlSi10Mg. *Acta Materialia*, 2016, vol. 117, pp. 311–320. DOI: 10.1016/j.actamat.2016.07.012.
20. Baitimerov R., Lykov P., Zherebtsov D., Radionova L., Shults A., Prashanth K. Influence of powder characteristics on processability of AlSi12 alloy fabricated by selective laser melting. *Materials*, 2018, vol. 11, p. 742. DOI: 10.3390/ma11050742.
21. Saprykina N.A., Chebodaeva V.V., Saprykin A.A., Sharkeev Y.P., Ibragimov E.A., Guseva T.S. Sintez trekh-komponentnogo splava na osnove alyuminiya metodom selektivnogo lazernogo plavleniya [Synthesis of a three-component aluminum-based alloy by selective laser melting]. *Obrabotka metallov (tekhnologiya, oborudovanie, instrumenty) = Metal Working and Material Science*, 2022, vol. 24, no. 4, pp. 151–164. DOI: 10.17212/1994-6309-2022-24.4-151-164.
22. Saprykina N.A., Chebodaeva V.V., Saprykin A.A., Sharkeev Y.P., Ibragimov E.A., Guseva T.S. Optimizatsiya rezhimov selektivnogo lazernogo plavleniya poroshkovoi kompozitsii sistemy AlSiMg [Optimization of selective laser melting modes of powder composition of the AlSiMg system]. *Obrabotka metallov (tekhnologiya, oborudovanie, instrumenty) = Metal Working and Material Science*, 2024, vol. 26, no. 1, pp. 22–37. DOI: 10.17212/1994-6309-2024-26.1-22-37.

Conflicts of Interest

The authors declare no conflict of interest.

© 2024 The Authors. Published by Novosibirsk State Technical University. This is an open access article under the CC BY license (<http://creativecommons.org/licenses/by/4.0>).